Title
Particle simulation of energetic particle driven Alfvén modes in NBI heated DIII-D experiments

Journal
Nuclear Fusion, 49(7)

ISSN
0029-5515

Authors
Vlad, G
Briguglio, S
Fogaccia, G
et al.

Publication Date
2009-07-01

DOI
10.1088/0029-5515/49/7/075024

Nucl. Fusion **49** (2009) 075024 (10pp) doi:10.1088/0029-5515/49/7/075024

Particle simulation of energetic particle driven Alfvén modes in NBI heated DIII-D experiments

G. Vlad, S. Briguglio, G. Fogaccia, F. Zonca, C. Di Troia, W.W. Heidbrink[1], M.A. Van Zeeland[2], A. Bierwage[1] and X. Wang[3]

Associazione EURATOM-ENEA, Frascati, Rome, Italy
[1] University of California, Irvine, CA, USA
[2] General Atomics, San Diego, CA, USA
[3] IFTS, Zhejiang University, Hangzhou, People's Republic of China

E-mail: gregorio.vlad@enea.it

Received 29 December 2008, accepted for publication 14 May 2009
Published 8 June 2009
Online at stacks.iop.org/NF/49/075024

Abstract
The mutual nonlinear interactions of shear Alfvén modes and alpha particles can enhance their transport in burning plasmas. Theoretical and numerical works have shown that rapid transport of energetic ions can take place because of fast growing Alfvén modes (e.g. energetic particle driven modes, EPMs). This kind of transport has been observed in experiments as well as in numerical simulations. Hybrid MHD-gyrokinetic codes can investigate linear and nonlinear dynamics of energetic particle (EP) driven modes, retaining the mutual interaction between waves and EPs self-consistently. Self-consistent nonlinear wave–particle interactions (both in configuration and velocity space) are crucial for a correct description of the mode dynamics in the case of strongly driven modes; thus, a non-perturbative approach is mandatory. The knowledge of the threshold characterizing the transition from weakly to strongly driven regimes is of primary importance for burning plasma operations (e.g. for ITER), in order to avoid EPM enhanced EP transport regimes. The hybrid MHD-gyrokinetic code (HMGC) has been applied to the interpretation of phenomena observed in present experiments with neutral beam (NB) heating. In reversed-shear beam-heated DIII-D discharges, a large discrepancy between the expected and measured EP radial density profiles has been observed in the presence of large Alfvénic activity. HMGC simulations with EP radial profiles expected from classical NB deposition as input give rise to strong EPM activity, resulting in relaxed EP radial profiles at saturation level close to experimental measurements. The frequency spectra obtained from several simulations with different toroidal mode numbers, as calculated during the saturated phase when the strong EPMs transform in weak reversed-shear Alfvén modes, are quite close to experimental observations both in absolute frequency and in radial localization. In this work, we discuss in particular the effects of nonlinear coupling between different toroidal mode numbers.

PACS numbers: 52.55.Pi, 52.35.Bj, 52.35.Lv, 52.50.Gj, 52.55.Fa

(Some figures in this article are in colour only in the electronic version)

1. Introduction

Transport of fast ions produced by fusion reactions and/or auxiliary heating can be enhanced by their resonant interaction with the Alfvén modes. Theoretical [1–4] and numerical work [5, 6] has shown, in particular, that rapid transport of fast ions can take place because of fast growing energetic particle driven modes (EPMs) [7]. EPMs have been proposed to generate 'avalanches', that is convectively amplified mode structures nonlinearly evolving on the same time scale of the ballistic fast-ion transport and following the radially moving unstable front; evidence of this phenomenology has also been observed, in fact, in numerical simulations [1]. Note that these nonlinear coherent dynamics are different in nature with respect to the case of multi-mode wave–particle interactions, for which the nonlinear resonant particle characteristics can locally exceed the Chirikov resonance overlap criterion [8] eventually causing stochastic diffusion in particle phase space, possibly because of a domino effect [9], producing fast-ion avalanches [10]. In this context, the single transport

events due to Alfvén eigenmodes (AEs) (avalanches) [10] may exhibit characteristic aspects of sandpile physics involving self-organized criticality (SOC) [11, 12]. A detailed discussion of differences and similarities of EPMs and AEs induced avalanches is given in [3] and will not be further analysed in this work.

Plasma regimes in which enhanced fast-ion transport occurs because of strongly driven EPMs should be avoided in order to reach reactor relevant performance and prevent first wall damage [2]. The investigation of the transition from regimes characterized by weakly driven modes (such as AEs, e.g. toroidal Alfvén eigenmodes, TAEs) to regimes dominated by strongly driven modes (like EPMs) and the determination of the related threshold are then of crucial importance for burning plasma operations. Hybrid MHD-particle codes are able to address these issues, as they retain particle–wave interactions in a self-consistent, non-perturbative, way.

The hybrid MHD-gyrokinetic code (HMGC [13]) has been used in the past [14] to predict both Alfvén mode and energetic particle dynamics in burning plasma scenarios (e.g. for ITER). In order to assess the reliability of these predictions, the code has to be validated with respect to the phenomena observed in present experiments, characterized by large fractions of fast ions. Such a validation has already been carried out for the case of negative neutral beam (NNB) heated JT-60U discharges. In these discharges, two types of bursting modes are observed by MHD spectroscopy [15]. The first one, called abrupt large-amplitude event (ALE), is characterized by a time scale of the order of 100 μs, a relatively large fluctuating magnetic field at the first wall, broad frequency spectra in the range of the Alfvén frequency and a significant decrease in the fast-ion density in the plasma centre. The second mode is observed during the relative quiescent phase between two consecutive ALEs. It is characterized by a longer time scale (few milliseconds), narrower frequency spectra, lower fluctuating field level and modest energetic-ion redistribution with respect to the ALE case. A peculiar characteristic of this mode is its chirping up and down in frequency: it has hence been dubbed fast frequency sweeping (FS) mode. Simulations performed by HMGC show [16] that the ALE dynamics can be explained in terms of the nonlinear behaviour of a fast growing EPM. The numerical simulation of the almost quiescent phase following ALEs compares well also with the fast FS phenomenology, provided that modifications of the fast-ion distribution function induced by the EPM saturation both in configuration (density profile) and in velocity space are retained and used as input to the ensuing HMGC run [16].

In this paper, we apply HMGC to the case of reversed-shear beam-heated DIII-D discharges. The plasma model adopted in HMGC consists of a thermal (core) plasma and an energetic-ion population. The former is described by reduced $O(\epsilon^3)$ MHD equations [17, 18] in the limit of zero pressure (ϵ being the inverse aspect ratio of the torus), including resistivity and viscosity terms; this model allows equilibria to be investigated with shifted circular magnetic surfaces only. The fast-ion population is described by the nonlinear gyrokinetic Vlasov equation [19, 20], expanded in the $k_\perp \rho_\mathrm{H} \ll 1$ limit (with $k_\perp$ the component of the wave vector perpendicular to the magnetic field and ρ_H the energetic-ion Larmor radius), but fully retaining magnetic drift orbit widths and solved by particle-in-cell (PIC) techniques. The gyrocentre Hamiltonian is retained up to $O(\epsilon_\mathrm{GK})$ terms, with ϵ_GK being the small parameter of the gyrokinetic ordering ($\rho_\mathrm{H}/a \sim \omega/\Omega_\mathrm{H} \sim e_\mathrm{H}\phi/m_\mathrm{H}v_\mathrm{H}^2 = O(\epsilon_\mathrm{GK})$, where Ω_H, e_H, m_H and v_H are, respectively, the Larmor frequency, charge, mass and typical velocity of energetic particles). This causes the total energy $\mathcal{E}$ to be conserved only up to the second order in ϵ_GK, $\mathrm{d}\mathcal{E}/\mathrm{d}t = O(\omega(e_\mathrm{H}\phi/m_\mathrm{H}v_\mathrm{H}^2)^2\mathcal{E}) = O(\epsilon_\mathrm{GK}^3\Omega_\mathrm{H}\mathcal{E})$, rather than to the next order, as for the usual gyrocentre treatment with Hamiltonian retained up to $O(\epsilon_\mathrm{GK}^2)$ terms [21]. Note, however, that this lack of conservation will not affect the validity of simulation results in a significant way. Indeed, both the linear growth rates and the nonlinear field saturation level are determined mainly by the retained dynamics, and the relative error on such quantities is $O(\epsilon_\mathrm{GK})$ due to Hamiltonian truncation at $O(\epsilon_\mathrm{GK})$. The coupling between energetic ions and thermal plasma is obtained through the divergence of the energetic-ion pressure tensor, which enters the vorticity equation [22]. Numerical simulations of experimental conditions are performed after fitting the relevant machine and thermal plasma quantities (the on-axis equilibrium magnetic field, major and minor radii (R_0 and a, respectively), the safety factor q, the electron n_e and ion n_i plasma densities, the electron temperature T_e), the fast-ion distribution function and the ratio β_H between fast ion and magnetic pressures.

The structure of the paper is the following: the main features of the experimental configuration considered and the corresponding setting of the numerical simulation are presented in section 2. In section 2.1, single toroidal mode number simulations are considered, which retain the nonlinear dynamics only through energetic particle nonlinear characteristics, while neglecting fluid mode–mode coupling between different toroidal mode numbers. It is shown that nonlinear effects of strongly unstable Alfvén modes can justify the discrepancy between the observed fast-ion density profile and that predicted by a classical neutral beam deposition model. Further comparisons between simulation results and the experimental observations are reported in section 2.2. In section 2.3, preliminary results of multi-mode simulations (including mode–mode coupling) of the same discharge considered in the previous sections are discussed. A summary and discussion are reported in section 3.

2. Numerical simulation of a reversed-shear beam-heated DIII-D discharge

A rich spectrum of oscillations in the Alfvénic frequency range has been observed in DIII-D tokamak discharges characterized by reversed-shear q-profile and heated by neutral beams [23]. During the phase of the discharge characterized by Alfvénic activity, the energetic particle density profile, calculated by a classical neutral beam deposition model (TRANSP code [24]), appears to be more peaked (cf figure 1) than that observed experimentally and inferred, e.g. from the fast-ion D_α (FIDA) diagnostic or from EFIT [25] equilibrium magnetic flux reconstructions using the motional Stark effect (MSE), magnetic measurements and thermal pressure data. In the latter case [23], the fast-ion pressure profile is inferred by subtracting the thermal plasma pressure profile, as obtained by electron,

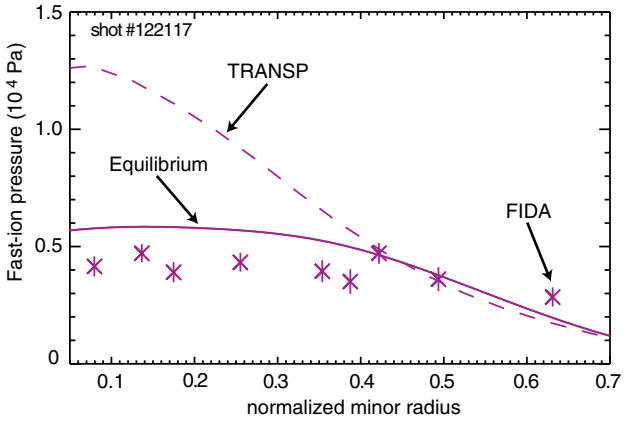

Figure 1. Fast-ion density profiles computed by TRANSP (dashed curve) compared with those inferred from the FIDA diagnostic (star symbols) or obtained by equilibrium reconstructions using MSE, magnetic measurements and thermal pressure data (solid curve).

bulk ion and carbon impurity measurements, from the MHD pressure profile as given by EFIT.

Here, we analyse shot #122117 at $t = 0.41\,\mathrm{s}$. The equilibrium configuration is characterized by $R_0 = 1.688\,\mathrm{m}$, $a = 0.609\,\mathrm{m}$, on-axis magnetic field $B_0 = 2\,\mathrm{T}$ and a reversed-q profile ($q_0 \approx 5$, $q_{\min} \approx 4$, $q_a \approx 10.5$). The initial energetic particle distribution function is assumed to have the following form:

$$F_0 = n(\psi)\, f_{\mathrm{sd}}(E, \psi)\Theta(\alpha, \alpha_0, \Delta). \tag{1}$$

Here $f_{\mathrm{sd}}(E, \psi)$ is a slowing down distribution function, with birth energy $E_0 = 0.077\,\mathrm{MeV}$ (in the experiment, 2/3 of the beams had birth energy of 0.075 MeV, and the remnant 1/3 had 0.081 MeV) and critical energy, depending on the poloidal magnetic flux coordinate ψ, given by the Stix formula [26]. The quantity Θ, given by

$$\Theta(\alpha, \alpha_0, \Delta) \equiv \frac{4}{\Delta\sqrt{\pi}} \frac{\exp\left[-\left(\dfrac{\cos\alpha - \cos\alpha_0}{\Delta}\right)^2\right]}{\mathrm{erf}\left(\dfrac{1-\cos\alpha_0}{\Delta}\right) + \mathrm{erf}\left(\dfrac{1+\cos\alpha_0}{\Delta}\right)}, \tag{2}$$

represents the anisotropy of the distribution function. In this expression, the following definitions have been used: $\cos\alpha \equiv v_\parallel/v$, with $v_\parallel$ being the parallel (to the magnetic field) component of the particle velocity v; $\alpha_0 \equiv \arccos(R_{\tan}/R_0) = \arccos(1.15\,\mathrm{m}/1.688\,\mathrm{m}) \approx 47^\circ$ is the injection angle, with $R_{\tan}$ and R_0 being the tangential radius of the beam and the major radius of the torus, respectively (cf figure 2); Δ is the width of the beam around $\cos\alpha_0$. The value of the parameter Δ can be inferred from the experimental ratio of the parallel to perpendicular energetic particle pressure $p_{\mathrm{par}}/p_{\mathrm{perp}} \approx 1.44$. Other numerical simulation parameters, fixed to match experimental conditions, are the on-axis fast ion $\beta_{\mathrm{H0}} \approx 0.8\%$ and the ratio between energetic and bulk ion masses is $m_{\mathrm{H}}/m_{\mathrm{i}} = 1$.

Note that this distribution function is not a function of invariants of fast particle motion only, and, in fact, it is not an equilibrium one. It is observed that the system evolves in a short time towards an equilibrium state, maintaining a small-amplitude level of oscillation around it. We conventionally indicate as *promptly relaxed* the state, close to the equilibrium, reached by the system in the short time transition. Figure 3 shows a measure of the variation of the energetic particle distribution function, proportional to $\int \mathrm{d}\boldsymbol{r}\,\mathrm{d}\boldsymbol{v}\,|F(\boldsymbol{r}, \boldsymbol{v}; t) - F_0(\boldsymbol{r}, \boldsymbol{v})|$ as a function of time, for a test simulation of the considered DIII-D case retaining only equilibrium dynamics: the promptly relaxed state is reached after $t \sim 200\omega_{\mathrm{A0}}^{-1}$, with $\omega_{\mathrm{A0}} \equiv v_{\mathrm{A0}}/R_0$ being the on-axis Alfvén frequency. Note that, within the same transient, also the phenomenon of the *first orbit* losses is almost completed, as shown in figure 4, where the total number of energetic particles (normalized to the value at $t\omega_{\mathrm{A0}} = 0$) is reported versus time, for the same simulation of figure 3.

In figure 5 the initial distribution function at a radial position around the maximum fast-ion density gradient and

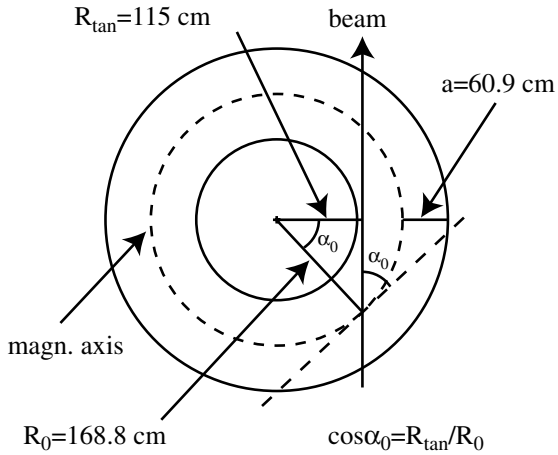

Figure 2. Sketch of the geometry of the beam injection.

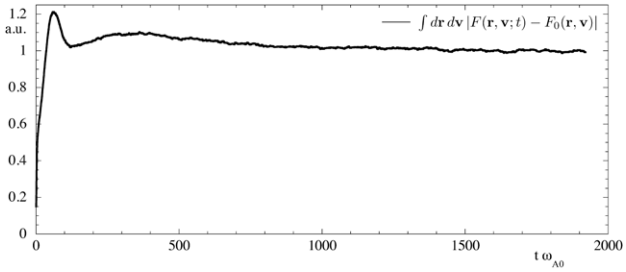

Figure 3. Variation of the energetic particle distribution function versus time. The distribution function relaxes to an equilibrium state after $t \sim 200\omega_{\mathrm{A0}}^{-1}$.

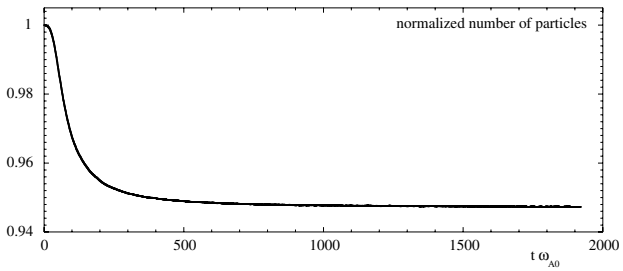

Figure 4. Total number of energetic particles versus time (normalized to the value at $t\omega_{\mathrm{A0}} = 0$).

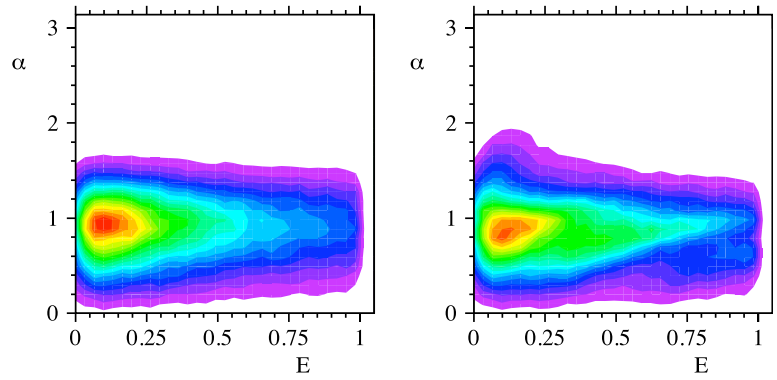

Figure 5. Initial (left) and promptly relaxed (right) distribution function in the (E, α) space at around the maximum fast-ion density gradient, averaged over the poloidal angle.

averaged over the poloidal angle is shown in the (E, α) space and compared with that of promptly relaxed state. This approach is not satisfactory in some cases, as the difference between the initialized energetic particle density profile and the promptly relaxed one can be quite relevant. Nonetheless, this representation was chosen since it allows an unambiguous reconstruction of the fast-ion distribution function from available experimental data, which correspond to density and temperature profiles given as functions of the poloidal flux ψ. There is no recipe to univocally determine which distribution function corresponds to these profiles in the space of invariants of fast particle motion. For example, the choice of lifting the profile dependences from ψ to the $(\psi, v_\parallel)$ space by substitution of $\psi \rightarrow P_\phi$ is expected to be adequate only in the small orbit width limit—that is, only in the limit in which even ψ nearly behaves like an invariant of fast particle motion. Meanwhile, equations (1) and (2) representation is asymptotically correct for large aspect ratio equilibria with small normalized fast-ion orbit widths with respect to the machine size. Despite the relaxation problem, this choice is transparent and—practically speaking—can well represent known aspects of experimental conditions. Further discussions on issues involved with representations of experimental profiles in the space of particle invariants of motion are given in [27] and will be reported in future publications. In the present work, these issues are not further discussed and the representation of equations (1) and (2) is assumed throughout.

2.1. Single toroidal mode number simulations

We first consider numerical results of single toroidal mode number simulations ($n = 2$–4, the dominant modes observed in the experiment), which fully retain energetic particle nonlinearities, while neglecting mode–mode coupling (the effects of this coupling will be addressed in section 2.3).

Assuming the fast-ion density profile resulting from TRANSP simulation as input for the HMGC simulation, strongly unstable modes are observed, which cause a violent redistribution of the fast ions for all the simulated toroidal mode numbers. In figure 6, the fast-ion profiles for such simulations are shown: the initialized TRANSP profile (black solid curve), the promptly relaxed profile as obtained after loading simulation particles according to equations (1) and (2)

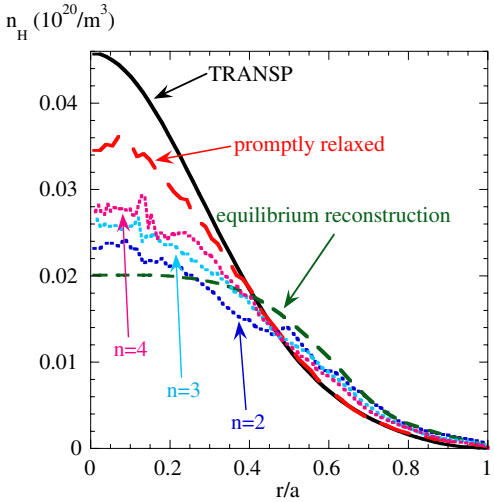

Figure 6. Fast-ion density profiles as computed by TRANSP (black solid curve), after the prompt relaxation (red long dashed curve), given by experimental equilibrium reconstruction (green dashed curve) and as obtained by the HMGC $n = 2, 3, 4$ simulations after nonlinear saturation (dotted curves).

(red long dashed curve) and the saturated profiles (dotted curves). The latter profiles are strongly modified with respect to the initial one, both in their central value and width; for $n = 2$, it is clearly close to the fast-ion profile obtained from equilibrium reconstruction, which is also reported for comparison (green dashed curve). In figure 7, the power spectra of the electrostatic potential during the linear growth (top) and the saturated phase (bottom) of the simulation are shown for the different toroidal mode numbers considered. Dominant modes are localized at the $q_{\min}$ radial position. Several very low-frequency modes are also observed in the saturated phase, which can be identified as resistive MHD modes, along with weaker Alfvén modes localized inside the toroidal gap (at least, in the $n = 4$ case). Concerning the low-frequency modes, note that they could be the result of an unphysically large resistivity required for numerics (not so large, however, to significantly affect Alfvén mode evolution); moreover, their dynamics could be affected by the fact that thermal ion kinetic compression due to geodesic curvature effects on shear Alfvén waves is not presently included in the code.

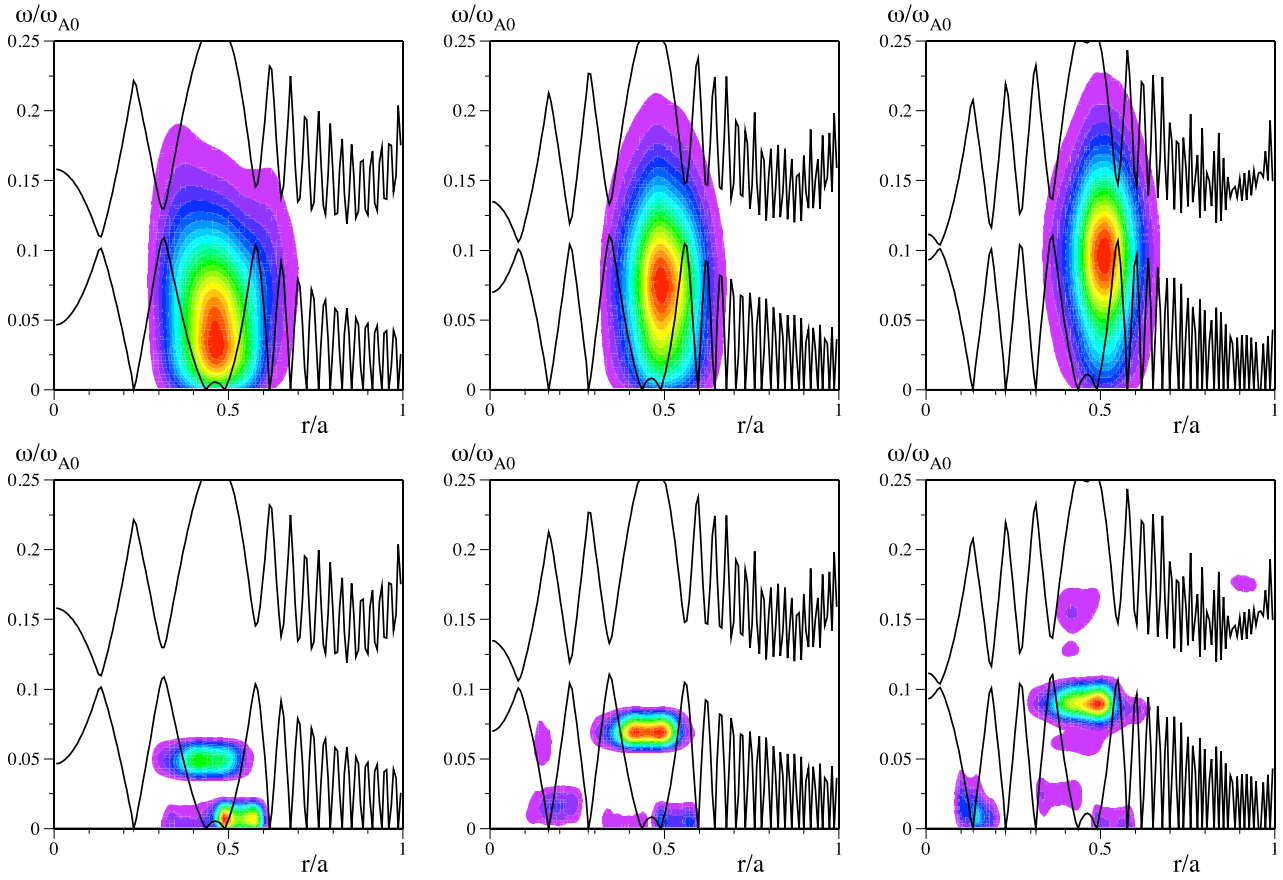

Figure 7. Power spectra of the scalar potential for $n = 2$ (left), $n = 3$ (centre) and $n = 4$ (right). The ordinate is ω/ω_{A0}, the Alfvén time in the centre being $\tau_{A0} \equiv \omega_{A0}^{-1} \approx 2.38 \times 10^{-7}$ s. The fast-ion initial density profile is from TRANSP. Top: linear phase, bottom: saturated phase. The Alfvén continuous spectrum corresponding to the considered n is also shown (black full curves).

From this set of simulations, we can draw the following conclusions: (a) the equilibrium profile computed by TRANSP, which neglects energetic particle collective excitations, is strongly unstable once Alfvén wave dynamics is accounted for; (b) the collective mode dynamics causes a relevant flattening of the energetic particle density profile; (c) the saturated state is close to that reconstructed experimentally (by EFIT and/or FIDA) and (d) the experimental profile could then be the consequence of a short time scale collective phenomenon.

We want to investigate whether the energetic particle distribution underlying the experimentally observed density profile (the profile labelled as 'equilibrium reconstruction' in figure 6) can be significantly different from a slowing down in the velocity space. For this reason, we have performed numerical simulations using a slowing down distribution as input with the quoted experimental fast-ion density profile. Figures 8 and 9, reporting the results of the $n = 2$ case, show that a sufficiently unstable mode still exists, saturating by a further relaxation of the energetic particle density profile, thus implying that the slowing down is not a good approximation of the more stable velocity space distribution function for the experimentally observed state. This is consistent with the above conclusion (d), taking into account that the saturation of a strongly unstable mode can significantly modify the energetic particle velocity space distribution function, besides their density profile [16]. Such a distortion is indeed observed in the simulation initialized with the TRANSP profile, as shown in figure 10: it effectively corresponds to a depletion of the resonant portion of the distribution function and, hence, to a lesser degree of instability.

It is important to observe, however, that no signatures of rapidly evolving EPMs have been observed to date in DIII-D discharges like that considered in this paper [23]. We will further discuss this issue in section 3.

2.2. *Comparison with measured electromagnetic fluctuations*

Assuming that the experimental fast-ion profile results from a short time scale collective phenomenon, we first compare qualitative and quantitative features of the experimentally observed frequency spectra of the modes with those predicted by the HMGC simulations initialized with the TRANSP profiles. In this respect, the main qualitative feature is certainly represented by the sensitive dependence of the mode frequency on the minimum-q value [23], which is typical of the so-called reversed-shear Alfvén eigenmodes (RSAEs) [28], also known as Alfvén cascades (AC) [29]. Figure 11 (top) shows the power spectra obtained for $n = 2$ for three different values of $q_{\min}$ during the linear mode growth. It is apparent that the frequency of the mode is weakly affected by the $q_{\min}$ variation and the corresponding modification of the Alfvén continuum. This is not surprising because the considered modes, in the linear phase, are strongly driven by energetic particles and, hence, their frequency is mainly determined by

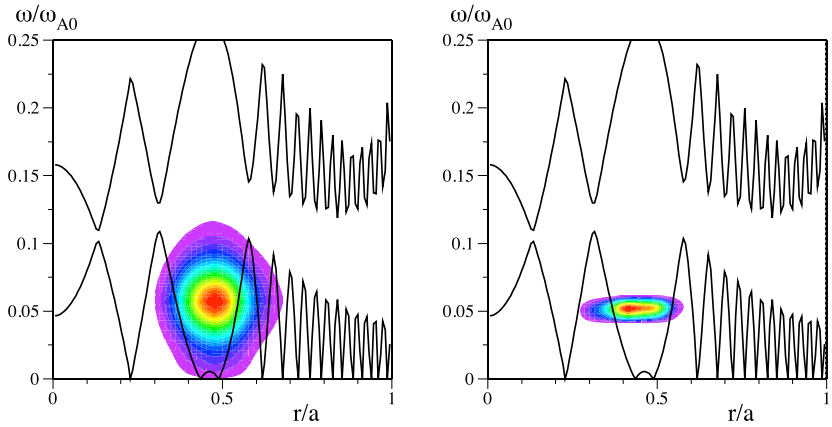

Figure 8. Power spectra of the electrostatic potential for a $n = 2$ simulation with an energetic particle density profile initialized according to the equilibrium reconstruction. Left: during the linear phase; right: during the saturated phase.

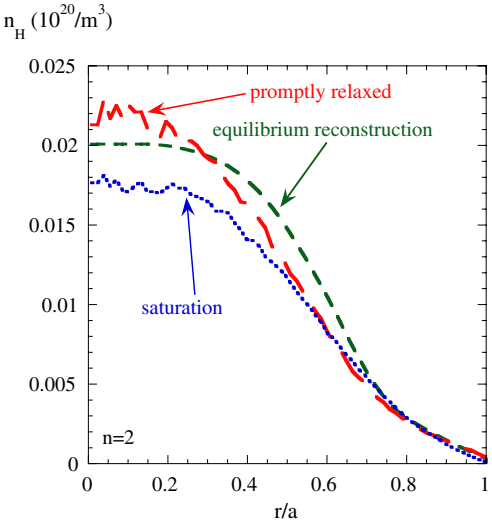

Figure 9. Energetic particle density profiles for the simulation considered in figure 8: the initialized profile from equilibrium reconstruction (green dashed curve), the promptly relaxed profile (red long dashed curve) and the saturated profile (blue dotted curve).

wave–particle resonance condition. After the large energetic particle redistribution (saturated phase), we expect that the weaker residual modes recover the experimentally observed dependence on $q_{\min}$ variations. This is confirmed by figure 11 (bottom).

From a quantitative point of view, the comparison between simulation results and experimental frequencies [30] is less satisfactory. This is not surprising, taking into account the strong dependence of the saturated mode frequency on $q_{\min}$ and the uncertainties in the determination of such quantity: a little difference in the MSE-based evaluation of q would imply a large difference in the saturated mode frequency resulting from the simulation. Indeed, the best agreement for the considered case is shown in figure 12, which refers to $q_{\min} \approx 3.89$ slightly smaller than the nominal value $q_{\min} \approx 4$, though well within the experimental error bars. Another factor that may cause the simulated frequencies to be below those of experiment is the lack of compressibility effects in the HMGC model. Indeed, finite thermal plasma pressure effects are most pronounced near the minimum of the RSAE frequency evolution (at $q_{\min} = 4$) and in fact can dominate the mode frequency [31]. Kinetic compression effects from thermal plasma ions and electrons are being implemented in a new version of HMGC, which will be able to address these issues.

Another interesting quantitative comparison between simulations and experiments concerns the amplitudes of the perturbed magnetic field. In the saturated phase of the $n = 2$ TRANSP-profile simulation considered in figure 7 (*left*) (nominal q profile), the value obtained at $r/a \approx 0.45$, where the mode is localized, are of order $\delta B_\theta / B_0 \approx 2.8 \times 10^{-3}$, $\delta B_r / B_0 \approx 3.5 \times 10^{-3}$. Those values are rather larger than the typical peak mode amplitudes inferred from MHD modelling, which are in the range $\delta B / B_0 \approx 5 \times 10^{-5}$–$5 \times 10^{-4}$. We shall address further this issue in the next section.

2.3. *Fully nonlinear multi-mode simulations*

The results described in the previous sections refer to single-mode simulations neglecting mode–mode coupling. The reasonable agreement between the fast-ion density profile found in numerical simulations after saturation and that measured experimentally can be considered as an indication that fast growing modes (not directly observed in the experiments) and their nonlinear interaction with energetic particles ultimately determine fast-ion profiles. In order to corroborate this hypothesis, however, we have to confirm that agreement persists once the simultaneous effect of all relevant toroidal modes is taken into account. For example, extending our single-n numerical analysis to the lower growth-rate toroidal numbers ($n = 1$ and $n = 5$) contiguous to those considered first, we find that $n = 1$ modes yield a displacement comparable to that obtained, e.g. in the $n = 2$ case, while the $n = 5$ modes produce negligible fast-ion displacement. This can be seen from figure 13, where the comparison between density profiles is presented, for these two cases, similarly to that shown in figure 6.

In this section, the preliminary results of a multi-mode $n = 0$–5 simulation (including mode–mode coupling) of the same discharge considered in the previous sections are presented. Some of nonlinear dynamics effects are still neglected; in particular, the evolution of the $m = 0$, $n = 0$ component of the fluctuating potentials is dropped, as well as that of the $m = 1$, $n = 0$ component of the fast-ion drive. The

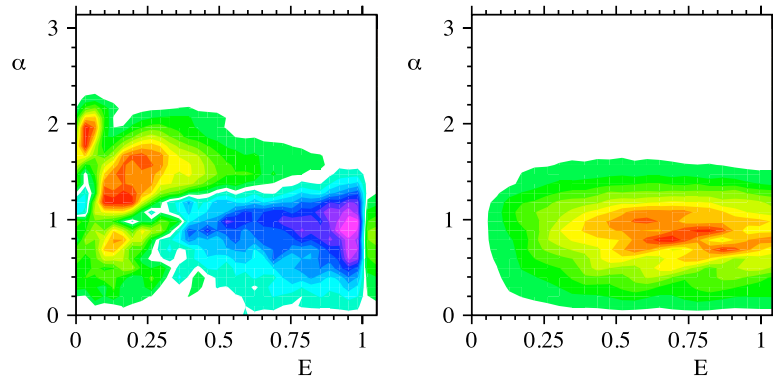

Figure 10. Distortion of the fast-ion distribution function induced by saturation of the fast growing mode, in the (E, α) space, for the $n = 2$ simulation with initial fast-ion density profile from TRANSP (left). The distortion is measured with respect to the promptly relaxed state, and averaged over toroidal and poloidal angles and a radial shell around the localization of the fast growing mode. Comparing this plot with that of an analogous average of the wave–particle power exchange (right), it is possible to observe that the nonlinear saturation of the mode causes a depletion of the distribution function in the resonance region. Depletion of the distribution function (left, region $0.25 \lesssim E \lesssim 1$ and $0 \lesssim \alpha \lesssim 1.4$) is represented by negative values (colours—electronic version only—from light blue to violet correspond to negative values; from light green to red correspond to positive ones). Wave-particle power exchange (right) only exploits positive values, i.e., power transferred from particles to wave (colours—electronic version only—from light green to red correspond to positive values).

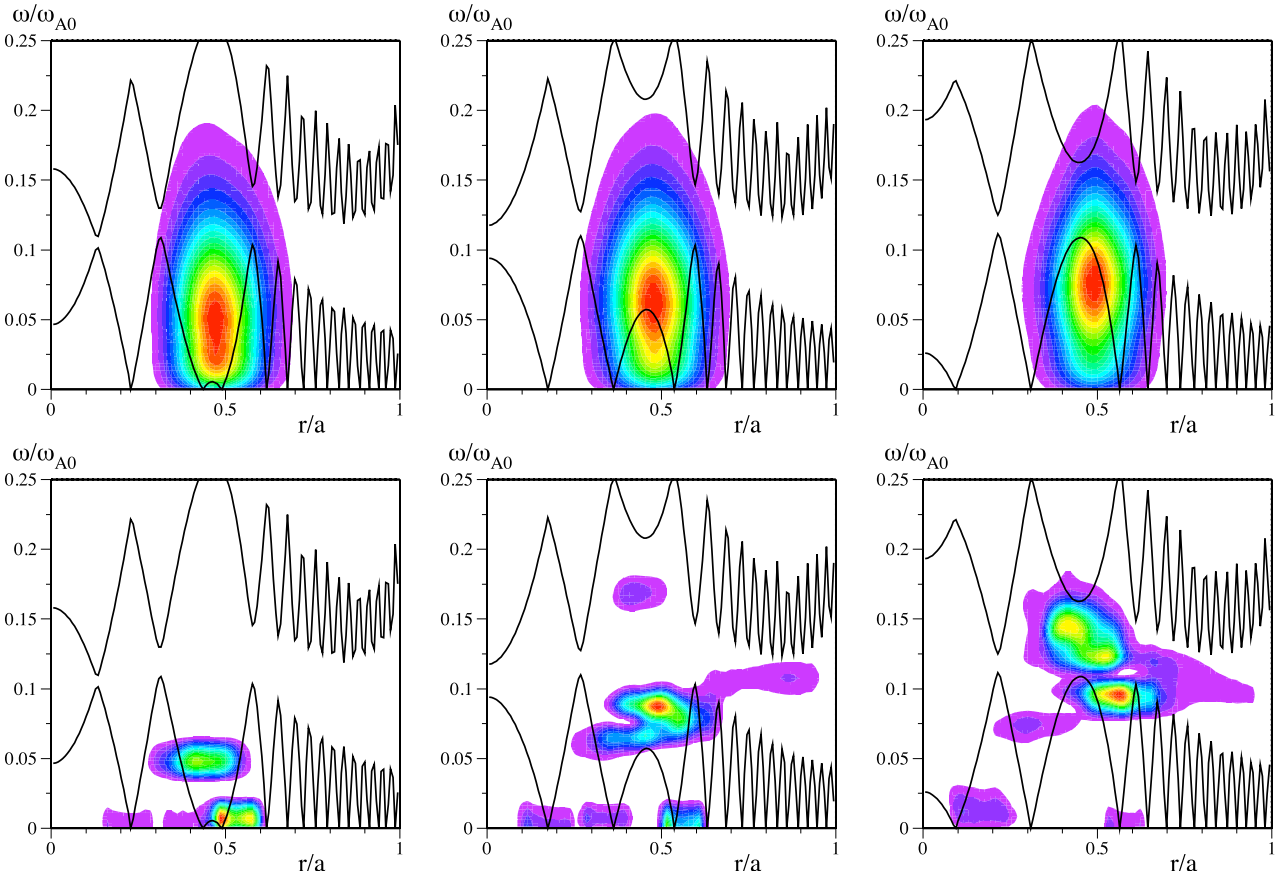

Figure 11. Power spectra for $n = 2$ and $q_{\min} = 3.99$ (nominal value, left), $q_{\min} = 3.89$ (centre) and $q_{\min} = 3.79$ (right) simulations initialized with the TRANSP fast-ion density profile. Top: linear phase; bottom: saturated phase.

reason for the former approximation is that the MHD model itself is not suited to properly describe the evolution of the $m = 0$, $n = 0$ equilibrium component. The aim of the latter is to avoid spurious dynamics effects due to the fact that the initial fast-ion distribution function is not expressed in terms of conserved quantities of particle motion.

Figure 14 shows the energy content of the dominant poloidal component for each of the retained toroidal numbers versus time. We note that in a first purely linear growth phase, modes with $n = 2$ and $n = 3$ exhibit the highest growth rates. As mode–mode coupling becomes important ($t \gtrsim 150\omega_{A0}^{-1}$), the interaction between $n = 2$ and $n = 3$ enhances the growth rate of $n = 5$ and, especially, $n = 1$ modes. This is easily understood in terms of three-wave nonlinear interactions. The $n = 2$ and $n = 3$ modes eventually saturate, giving rise to fast-ion displacement ($t \approx 190\omega_{A0}^{-1}$).

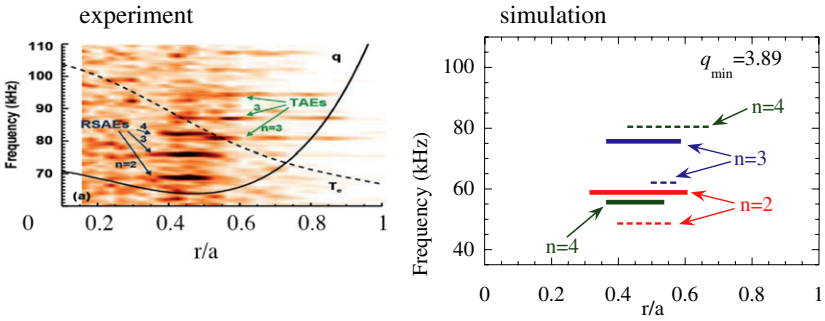

Figure 12. An experimental frequency spectrum (left) and single-n simulation results (right) with a slightly modified ($q_{\min} = 3.89$) safety factor profile (two modes for each n are shown: the dominant ones—thick continuous lines and the subdominant ones—thin dashed lines); the radial extension of the lines indicates the radial mode width.

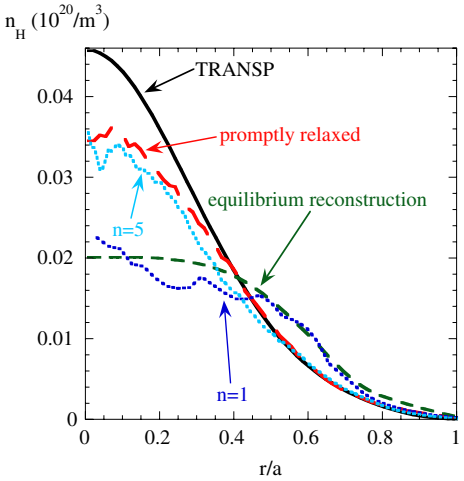

Figure 13. Saturated fast-ion profiles obtained in single-n simulations for toroidal numbers $n = 1$ (blue dotted curve) and $n = 5$ (light blue dotted curve), compared with the initial profile (that obtained from the TRANSP simulation, black solid curve), the promptly relaxed one (red long dashed curve) and the experimental equilibrium reconstruction (green dashed curve).

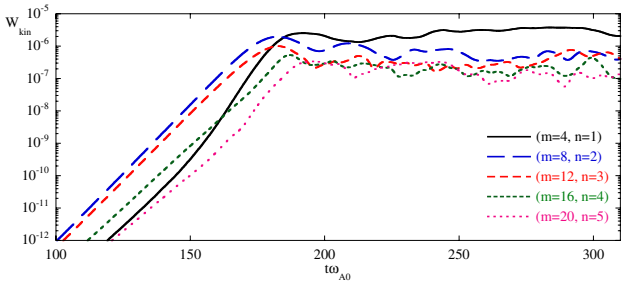

Figure 14. Fully nonlinear multi-mode simulation: kinetic energy content of the dominant poloidal harmonics for different n values.

The $n = 1$ mode, once the drive due to three-wave coupling is exhausted, is still driven by the residual fast-ion pressure gradient. Then, it further grows ($t \gtrsim 200\omega_{A0}^{-1}$) and eventually produces further ion density flattening, reaching saturation itself ($t \gtrsim 370\omega_{A0}^{-1}$). Figure 15 presents the power spectra of the scalar potential during the linear growth phase (top) and after complete saturation (bottom) for the multi-mode simulation. Global (all n) power spectra (left) are compared with the $n = 1$ (centre) and $n = 2$ (right) ones. The linear-growth phase is dominated by the $n = 2$ mode, while the $n = 1$ mode prevails in the saturated phase.

The overall effect on the fast-ion density profile is of the same order of that obtained in single-mode simulations (see figure 16, left). In the present case, both competition of different-n modes in extracting energy from resonant particles (as expected for EPMs), thereby flattening the fast-ion profile, and the energy transfer from fast to slower growing modes by three-wave nonlinear interactions cause each toroidal mode to saturate at a lower level than that reached in the corresponding single-mode simulation. This is shown in figure 16, right, which compares the saturation levels obtained, in single-mode and multi-mode simulations, for the dominant poloidal harmonics of the poloidal electric field (responsible for fast-ion convective displacement) corresponding to different n values. The observed reduction of the saturation levels goes in the direction of better agreement between perturbed field levels predicted by numerical simulations and those inferred from MHD modelling.

The results of multi-mode simulations, presented here, indicate that the low-frequency $n = 1$ mode, in the saturated phase, is even more relevant than the experimentally observed modes $n = 2$–4, in spite of its lower linear growth rate. Note, however, that such a conclusion could be strongly dependent on the detailed structure of the low-frequency structure of the Alfvén continuum. Such a structure could be modified both because of slight variations of the $q_{\min}$ value (cf figure 11) as well as including additional physics in the model. In particular, the $O(\epsilon^3)$ reduced MHD equations in the zero-β_{bulk} approximation neglect sound waves and geodesic curvature couplings. If such effects were properly retained [2, 3, 32, 33], a kinetic thermal ion frequency gap is formed [3], where beta induced Alfvén eigenmodes (BAEs) could exist [34, 35]. As discussed above, these physics are being implemented in a new version of HMGC via a kinetic hybrid scheme and will be the subject of future investigations.

3. Summary and discussion

The HMGC code has been applied to the simulation of a reversed-shear beam-heated DIII-D discharge (#122117) that exhibits an intense Alfvénic activity. During such activity, the fast-ion density profile is broader than that computed

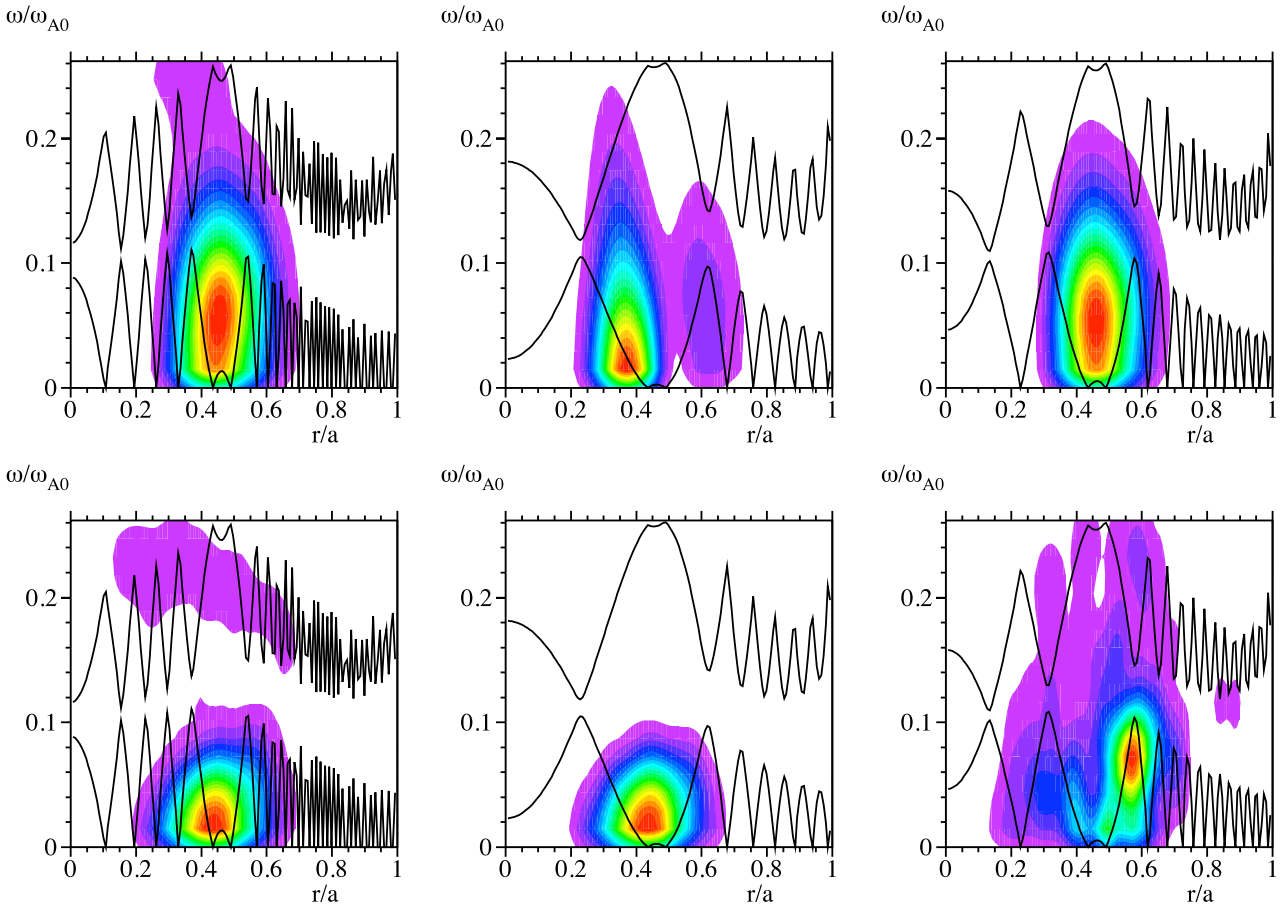

Figure 15. Fully nonlinear multi-mode simulation. Top: frequency spectra in the linear phase for all toroidal mode numbers (left), only $n = 1$ (centre), only $n = 2$ (right). Bottom: frequency spectra during the saturated phase for all toroidal mode numbers (left), only $n = 1$ (centre), only $n = 2$ (right). The Alfvén continuous spectra for $n = 5$ (left frames), $n = 1$ (centre frames) and $n = 2$ (right frames) are also shown, respectively.

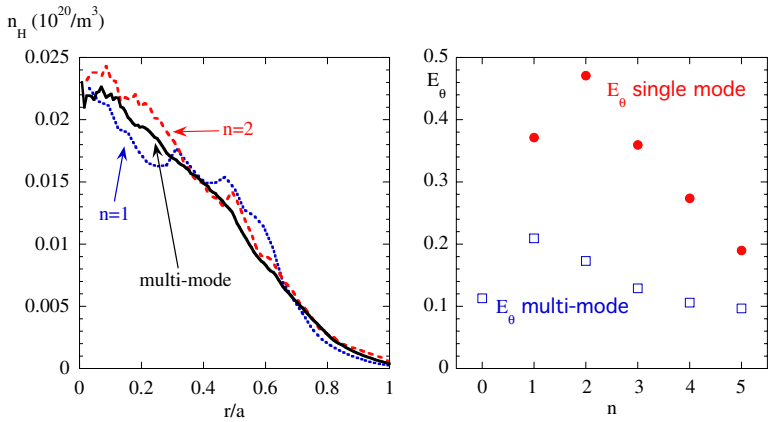

Figure 16. Energetic particle density profiles at saturation (left) and saturation levels of the poloidal electric field (right) of the fully nonlinear multi-mode simulation compared with those of single-n simulations.

by the TRANSP code, on the basis of a classical neutral beam deposition model. Simulation results suggest a possible interpretation of this discrepancy. In fact, they show that the fast-ion profile computed by TRANSP is strongly unstable because of fast growing Alfvén modes localized around the minimum q position. The nonlinear saturation of these modes is accompanied by a marked flattening of the fast-ion density profile, which is close to that observed in the experiments. A relevant distortion of the fast-ion distribution function also occurs in the velocity space, corresponding to a depletion of the resonant particle population. These results show why the experimentally observed profile is so different from the classically computed one: the latter is not compatible with the dynamics generated by wave–particle interactions.

We can also conjecture that the experimentally observed configuration can be interpreted as the saturated state of a short

time scale collective phenomenon, partially reconstructed by the continuous beam fuelling. To corroborate this hypothesis, we have compared the main features of fluctuation spectra predicted by the simulation and those deduced from experimental data. Some of these features are reasonably well reproduced (frequency range and sensitivity to the variation of $q_{\min}$, radial localization); others, the amplitude of the perturbed magnetic field in particular, are more problematic and suggested more comprehensive numerical analyses. Concerning the latter issue, the agreement for the amplitude of each toroidal component of the fluctuating field is improved with respect to the case of single-mode studies once multi-mode simulations (including mode–mode coupling) are performed.

No evidence of fast growing EPMs has been so far observed, however, in DIII-D discharges. This fact may suggest that a low level Alfvén mode activity induced by the continuous beam fuelling prevents the system from developing a violently unstable distribution function (like the TRANSP one, assumed as input in our simulation). If this were the case, neither fast growing modes would occur nor, correspondingly, dramatic distortions in the velocity space distribution function. In this respect, it is important to remind the reader of a substantial caveat: there is a fundamental difference between simulating a continuous beam fuelling that pushes the system through the threshold condition for mode excitation and setting up a given initial fast-ion distribution function that self-consistently evolves in the presence of fluctuations but without sources and sinks. Self-consistent numerical simulations treating fast-ion sources and sinks on the same footing of fluctuation induced transport processes and nonlinear Alfvén mode dynamics are necessary for progressing further in this area. This is presently beyond the capability of particle simulation codes, as it requires extending simulations beyond the transport time scale, which is much longer than the Alfvén-mode nonlinear characteristic time. The fundamental interest in this problem, for both its theoretical relevance and practical impact, makes it one of the main challenges for fusion research in the near future.

On the other hand, strong redistribution of the fast-ion population has been detected in NNB heated JT-60U discharges and related to the presence of EPMs. It then seems inappropriate to generally exclude that fast collective phenomena can play an important role in the dynamics of plasmas characterized by a large fraction of energetic particles. The relative importance of nonlinear Alfvén mode dynamics, the partial reconstruction due to the fast-ion source, the sampling rate connected with the intrinsic time resolution of the diagnostic systems in determining the effective time scale of the observed phenomena and the identification of the relevant parameters for a transition from weak to strong nonlinear dynamics have to be considered open and major issues in the research on fast-ion effects in burning plasmas.

References

[1] Zonca F., Briguglio S., Chen L., Fogaccia G. and Vlad G. 2005 *Nucl. Fusion* **45** 477–84
[2] Zonca F., Briguglio S., Chen L., Fogaccia G., Hahm T.S., Milovanov A.V. and Vlad G. 2006 *Plasma Phys. Control. Fusion* **48** B15–28
[3] Chen L. and Zonca F. 2007 *Nucl. Fusion* **47** S727–34
[4] Chen L. 2008 *Plasma Phys. Control. Fusion* **50** 124001
[5] Briguglio S., Zonca F. and Vlad G. 1998 *Phys. Plasmas* **5** 3287–301
[6] Todo Y., Nakajima N., Shinohara K., Takechi M., Ishikawa M. and Yamamoto S. 2004 Nonperturbative effects of energetic ions on Alfvén eigenmodes *Proc. 20th Int. Conf. on Fusion Energy 2004 (Vilamoura, Portugal, 2004)* (Vienna: IAEA) CD-ROM file TH/3-1Ra and http://www-naweb.iaea.org/napc/physics/fec/fec2004/datasets/index.html
[7] Chen L. 1994 *Phys. Plasmas* **1** 1519–22
[8] Chirikov B.V. 1979 *Phys. Rep.* **52** 263–379
[9] Berk H.L. *et al* 1996 *Phys. Plasmas* **3** 1827–38
[10] Berk H.L. *et al* 1995 *Nucl. Fusion* **35** 1661–8
[11] Bak C., Tang C. and Wiesenfeld K. 1987 *Phys. Rev. Lett.* **59** 381–4
[12] Dendy R.O. and Helander P. 1997 *Plasma Phys. Control. Fusion* **39** 1947–62
[13] Briguglio S., Vlad G., Zonca F. and Kar C. 1995 *Phys. Plasmas* **2** 3711–23
[14] Vlad G., Briguglio S., Fogaccia G., Zonca F. and Schneider M. 2006 *Nucl. Fusion* **46** 1–16
[15] Shinohara K. *et al* 2004 *Plasma Phys. Control. Fusion* **46** S31–45
[16] Briguglio S., Fogaccia G., Vlad G., Zonca F., Shinohara K., Ishikawa M. and Takechi M. 2007 *Phys. Plasmas* **14** 055904
[17] Strauss H.R. 1977 *Phys. Fluids* **20** 1354–60
[18] Izzo R., Monticello D.A., Park W., Manickam J., Strauss H.R., Grimm R. and McGuire K. 1983 *Phys. Fluids* **26** 2240–6
[19] Frieman E.A. and Chen L. 1982 *Phys. Fluids* **25** 502–8
[20] Lee W.W. 1987 *J. Comput. Phys.* **72** 243–69
[21] Brizard A.J. and Hahm T.S. 2007 *Rev. Mod. Phys.* **79** 421–68
[22] Park W. *et al* 1992 *Phys. Fluids* B **4** 2033–7
[23] Heidbrink W.W. *et al* 2008 *Nucl. Fusion* **48** 084001
[24] Budny R.V. *et al* 1995 *Nucl. Fusion* **35** 1497–508
[25] Lao L.L. *et al* 1985 *Nucl. Fusion* **25** 1611–22
[26] Stix T.H. 1972 *Plasma Phys.* **14** 367–84
[27] Bierwage A. *et al* 2008 *Bull. Am. Phys. Soc.* **53** 75
[28] Takechi M. *et al* 2002 Property of Alfvén eigenmode in JT-60U reversed shear and weak shear discharges *Proc. 19th Int. Conf. onFusion Energy 2002 (Lyon, France, 2002)* (Vienna: IAEA) CD-ROM file EX/W-6 and http://www.iaea.org/programmes/ripc/physics/fec2002/html/fec2002.htm
[29] Sharapov S.E. *et al* 2001 *Phys. Lett.* A **289** 127–34
[30] Van Zeeland M.A., Kramer G.J., Austin M.E., Boivin R.L., Heidbrink W.W., Makowski M.A., McKee G.R., Nazikian R., Solomon W.M. and Wang G. 2006 *Phys. Rev. Lett.* **97** 135001
[31] Van Zeeland M.A. *et al* 2008 *Plasma Phys. Control. Fusion* **50** 035009
[32] Zonca F., Chen L. and Santoro R.A. 1996 *Plasma Phys. Control. Fusion* **38** 2011–28
[33] Zonca F. and Chen L. 2006 *Plasma Phys. Control. Fusion* **48** 537–56
[34] Turnbull A.D. *et al* 1993 *Phys. Fluids* B **5** 2546–53
[35] Heidbrink W.W., Strait E.J., Chu M.S. and Turnbull A.D. 1993 *Phys. Rev. Lett.* **71** 855–8